PHYSICAL REVIEW E **87**, 050301(R) (2013)

Chiral diffusion of rotary nanomotors

Amir Nourhani,[1,2] Paul E. Lammert,[2,*] Ali Borhan,[1] and Vincent H. Crespi[2,†]
[1]*Department of Chemical Engineering, The Pennsylvania State University, University Park, Pennsylvania 16802, USA*
[2]*Department of Physics, The Pennsylvania State University, University Park, Pennsylvania 16802, USA*
(Received 26 June 2012; revised manuscript received 23 December 2012; published 8 May 2013)

Neither a purely deterministic rotary nanomotor nor a purely orientational diffuser exhibits long-term translational motion, but coupling rotation to orientational diffusion yields translational diffusion. We demonstrate that this effective translational diffusion can easily dominate the ordinary thermal translational diffusion for experimentally relevant nanomotors, and that this effective diffusion is *chiral*. Unpowered chiral particles do not exhibit chiral diffusion, but a nanorotor has both handedness and an instantaneous direction of powered motion, thus—unlike an unpowered particle—its diffusional motion can distinguish left from right.

DOI: 10.1103/PhysRevE.87.050301 PACS number(s): 82.70.Dd, 47.63.mf, 05.40.−a

The development of artificial nanomotors that move autonomously by transducing chemical energy to mechanical motion has defined a fascinating new field in colloid science [1–5]. Many models explain *deterministic* motion of various linear nanomotors [5–9]. However, the significance of thermal fluctuations at the nanoscale raises important questions about how deterministic and stochastic dynamics interact for powered objects [10,11]. Whereas translational and orientational Brownian diffusion are weakly coupled for ordinary unpowered colloidal nanorods—even under external driving—for *nanomotors* the direction of powered motion can be strongly influenced by a stochastic orientation. This interplay is of fundamental interest, but is also important to the interpretation of experimental data and designing motors.

Previously, Lauga [12] (see also Ref. [13]) considered coupling of orientational diffusion to powered linear motion in three dimensions with a cyclic speed schedule, and van Teeffelen and Löwen [14] analyzed a planar rotor. Here we demonstrate that the coupling of orientational diffusion with powered rotation in a nanorotor creates an effective translational diffusion with medium-term *chiral* bias: The motor is not equally likely to wander left or right from its position during one period; chiral symmetry of traditional diffusion is broken.

Imagine a nondiffusing powered rotor and an unpowered purely orientational diffuser. Neither exhibits translational diffusion. However, when a powered nanorotor experiences orientational diffusion, that stochastic motion deforms its deterministic circular path (see Fig. 1), resulting in an effective translational diffusion at long times. A nanorotor near a flat substrate (the typical experimental geometry) moves in a plane at speed v in a direction which rotates at a deterministic constant angular velocity ω and wanders stochastically with orientational diffusion coefficient D_o. For a linear nanomotor (i.e., with $\omega = 0$), the induced effective diffusion represents a degradation of the ability to get from one place to another, but for a *nanorotor* the effect is opposite. We derive the effective diffusion coefficient D_{eff} in terms of the fundamental parameters D_o, v, and ω, similar to the results given in Refs. [11,15,16]. D_{eff} is an asymptotic property. We extend the analysis to short-time correlations through stroboscopic sampling of the motion at integer multiples of the period. Under this sampling, the purely deterministic rotary motion is invisible, but a chirality manifests: The expected displacement after one period has a chirality-dependent component that can be comparable to the orbit radius. A powered nanorotor has both a handedness and an instantaneous direction of motion, thus its diffusional motion can distinguish left from right.

As illustrated in Fig. 1, the particle follows an instantaneous circular trajectory of radius $R = v/\omega$ about an instantaneous center $\boldsymbol{c}(t)$. The particle's laboratory-frame position $\boldsymbol{x}(t)$ and its location $\boldsymbol{p}(t)$ in the moving frame with origin at $\boldsymbol{c}(t)$ are related by $\boldsymbol{x}(t) = \boldsymbol{c}(t) + \boldsymbol{p}(t)$. In the absence of orientational Brownian motion ($D_o = 0$), $\boldsymbol{c}$ is constant. With two-dimensional vectors represented as complex numbers, the particle's location with respect to $\boldsymbol{c}(t)$ is $\boldsymbol{p}(t) = R\boldsymbol{u}(t) = Re^{i\theta(t)}$ and its instantaneous velocity is $\boldsymbol{v} = iv\boldsymbol{u}$. The change in position $\boldsymbol{x}$ for an infinitesimal time dt is

$$d\boldsymbol{x} = iv\,\boldsymbol{u}\,dt. \tag{1}$$

The particle orientation evolves according to the stochastic differential equation $d\theta = \omega\,dt + \sigma\,dW$, where $\sigma = \sqrt{2D_o}$ and $W(t)$ is a normalized Wiener process: $W(t) - W(t')$ is normally distributed with mean zero and variance $|t - t'|$, and increments for nonoverlapping intervals are independent. The orientation, central to later calculations, is

$$\boldsymbol{u}(t) = e^{i[\omega t + \sigma W(t)]}. \tag{2}$$

The velocity autocorrelation function, measuring how rapidly the motor forgets its orientation, is the same as the $\boldsymbol{u}$ autocorrelation function up to a constant factor v^2. It follows from Eq. (2) and $\langle e^{i\sigma[W(t)-W(t')]}\rangle = e^{-\sigma^2|t-t'|/2}$ that

$$C_{\boldsymbol{u}\boldsymbol{u}^*}(t) := \langle \boldsymbol{u}(t)\boldsymbol{u}(0)^*\rangle = e^{i\omega t - D_o|t|}, \tag{3}$$

where the orientational correlation time is $D_o^{-1} = 2/\sigma^2$. The angled brackets average over both the initial orientation $\boldsymbol{u}(0)$ and perturbation realization W. The orientation becomes scrambled after about $(2\pi|\tau|)^{-1}$ orbits, where $|\tau|$ is the ratio of the deterministic time scale $|\omega|^{-1}$ to the orientation correlation time D_o^{-1}, i.e., $\tau = \omega^{-1}/D_o^{-1} = \sigma^2/2\omega$. The parameters ω, v, and τ are all signed quantities to allow for both chiralities. The loss of orientational correlation drives long-term diffusive

*pel1@psu.edu
†vhc2@psu.edu

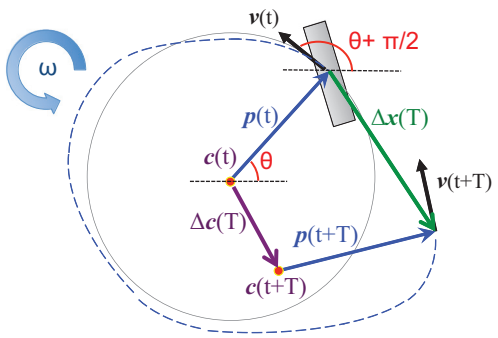

FIG. 1. (Color online) At time t, the nanorotor orbits at velocity $\boldsymbol{v}(t)$ about a guiding center $\boldsymbol{c}(t)$, with position $\boldsymbol{p}(t)$ relative to that center. Orientational diffusion deforms the trajectory. One cycle T later, the motor is instantaneously on a circular trajectory about a new center $\boldsymbol{c}(t+T)$. The velocity and motor axis do not necessarily align.

behavior for both the particle position $\boldsymbol{x}$ and the guiding center $\boldsymbol{c}$.

The effective diffusion coefficient does not depend on the initial conditions on $\boldsymbol{u}$, since they are forgotten exponentially fast. Using the Green-Kubo formula in two dimensions combined with Eqs. (1) and (3) leads to $D_{\rm eff} = \lim_{t\to\infty} \frac{1}{2}\int_0^t \langle \vec{v}(t)\cdot \vec{v}(0)\rangle\, dt = v^2\,{\rm Re}\{\int_0^\infty dt'\, C_{\boldsymbol{u}\boldsymbol{u}^*}(t')\}$, where Re extracts the real part; hence,

$$D_{\rm eff} = \frac{v^2}{2\omega}\left(\frac{\tau}{1+\tau^2}\right). \tag{4}$$

A one-dimensional diffusional process—orientational diffusion in a fixed plane—generates two-dimensional translational diffusion through coupling to powered motion. The effective diffusion coefficient $D_{\rm eff}$, represented by the thick solid gray curve in Fig. 2, varies nonmonotonically with $D_{\rm o}$ and attains a peak value of $v^2/4|\omega|$ for $|\tau| = 1$, when the deterministic and stochastic time scales are equal. Both $\boldsymbol{x}$ and $\boldsymbol{c}$ have the same effective diffusion coefficient, owing

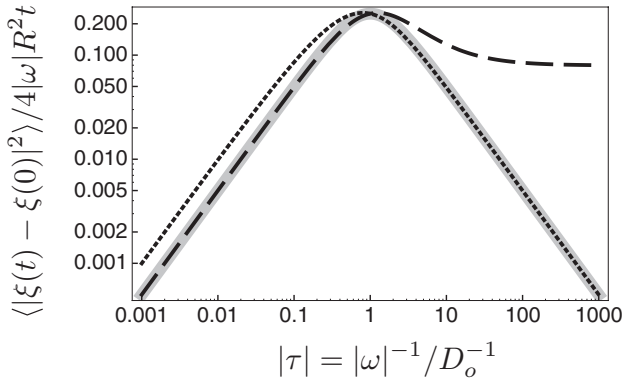

FIG. 2. Dimensionless mean square increments across one period of the rotation, $\langle|\boldsymbol{\xi}(T)-\boldsymbol{\xi}(0)|^2\rangle/4|\omega|R^2T$, for the center of mass $\boldsymbol{\xi} = \boldsymbol{x}$ (dotted) and the center of rotation $\boldsymbol{\xi} = \boldsymbol{c}$ (dashed). The gray curve shows the $t\to\infty$ common asymptotic behavior of $\boldsymbol{x}$ and $\boldsymbol{c}$, i.e., $D_{\rm eff}/|\omega|R^2 = \lim_{n\to\infty}\langle|\boldsymbol{\xi}(nT)-\boldsymbol{\xi}(0)|^2\rangle/4|\omega|R^2nT$ as the effective translational diffusion coefficient. The deviations above the asymptote indicate anticorrelations between changes of $\boldsymbol{\xi}$ across periods, as depicted in Fig. 3.

to the constraint $|\boldsymbol{c}-\boldsymbol{x}| = R$. However, their motions differ markedly across one period $T = 2\pi|\omega|^{-1}$ of the deterministic rotation: $\langle|\boldsymbol{\xi}(T)-\boldsymbol{\xi}(0)|^2\rangle/T$ for $\boldsymbol{\xi} = \boldsymbol{x}$ and $\boldsymbol{\xi} = \boldsymbol{c}$ both deviate from $4D_{\rm eff}$, but in different regimes, as shown in Fig. 2.

To develop our intuition, consider the limiting regimes of fast and slow orientational diffusion. For $|\tau| \gg 1$, the particle forgets its orientation so rapidly that the deterministic rotational motion is irrelevant. It might as well be moving straight at speed v, except that its direction changes after time $D_{\rm o}^{-1}$. Thus, it follows a random walk with steps of length $v/D_{\rm o}$ and duration $D_{\rm o}^{-1}$. The diffusion coefficient $D_{\rm eff} \approx v^2/2D_{\rm o}$ is proportional to (step length)^2/(step duration) and independent of ω. In this regime, $\boldsymbol{x}$ barely moves and $\boldsymbol{c}$ diffuses rapidly on a circle centered at $\boldsymbol{x}$, which explains why $\langle|\boldsymbol{x}(T)-\boldsymbol{x}(0)|^2\rangle/T$ is very close to $4D_{\rm eff}$ when $|\tau| \gg 1$, whereas $\langle|\boldsymbol{c}(T)-\boldsymbol{c}(0)|^2\rangle/T$ is much larger. Motion on a circle cannot contribute to long-term diffusion.

When the stochastic time scale is much larger than the deterministic time scale ($|\tau| \ll 1$), $D_{\rm eff} \approx v^2D_{\rm o}/2\omega^2$ is linear in $D_{\rm o}$. In this regime, the circular orbit is only slightly perturbed. In a short time interval Δt, the random change in orientation ($\sim\sqrt{D_{\rm o}\Delta t}$) leads to a random shift $|\Delta\boldsymbol{c}| \sim R\sqrt{D_{\rm o}\Delta t}$ (recall that $\boldsymbol{c}$ is not moved by the deterministic orientation change). The random walk formula gives a diffusion coefficient for $\boldsymbol{c}$ proportional to $R^2D_{\rm o} = v^2D_{\rm o}/\omega^2$. The random motion of $\boldsymbol{c}$ is always on a circle about the position $\boldsymbol{x}$, but in this regime $\boldsymbol{c}$ changes only a little before $\boldsymbol{u}$ has changed significantly, causing the curvature of the motion about $\boldsymbol{x}$ to disappear. Therefore, this motion is nearly along a time-dependent axis, and $\langle|\boldsymbol{c}(T)-\boldsymbol{c}(0)|^2\rangle/T$ closely follows $4D_{\rm eff}$.

Is this effective diffusion a significant contributor to the overall translational diffusion of real nanorotors? For a typical "slow" rotor [17], $\omega^{\rm slow} \approx 2.3$ rad/s and $D_{\rm o}^{\rm slow} \approx 0.1$ rad^2/s, while for a typical "fast" rotor [18], $\omega^{\rm fast} \approx 30$ rad/s and $D_{\rm o}^{\rm fast} \approx 0.5$ rad^2/s. Both nanorotors operate in the regime of weak orientational diffusion, $|\tau| \equiv |\omega|^{-1}/D_{\rm o}^{-1} \ll 1$. The linear velocity of the slow nanomotor is $v^{\rm slow} \sim 10$ μm/s [19], which yields an effective diffusion coefficient of $D_{\rm eff}^{\rm slow} \simeq 0.9$ μm^2/s. For the fast rotor, $v^{\rm fast} \sim 30$ μm/s [20] and $D_{\rm eff}^{\rm fast} \simeq 0.2$ μm^2/s. The passive translational diffusion coefficient for a similarly sized (2 μm long) unpowered nanorod in water is about $D_{\rm t} = 0.4$ μm^2/s [19]. For the slow rotor, the effective diffusion is twice as strong as passive translational diffusion. More generally, when orientational diffusion is weak (i.e., $\tau \ll 1$), $D_{\rm eff}$ scales linearly in $D_{\rm o}$. Since $D_{\rm t} \propto L^{-1}$ but $D_{\rm o} \propto L^{-3}$, the ratio of the effective roto-Brownian diffusion to passive translational diffusion scales as L^{-2}. Thus, for typical nanorotors synthesized to date, effective diffusion can dominate at sub-μm scales.

Over long times compared to the period of rotation and the orientational correlation time, the effects of chirality wash out, since the phase of the nanorotor in its orbit randomizes. However, the effective diffusion over shorter times can strongly manifest chirality. The short-time diffusion can be seen most clearly by examining the motion stroboscopically at multiples of $T = 2\pi\omega^{-1}$, the period of the deterministic rotation. This sampling makes the deterministic part of the motion invisible.

The displacement expectations for short times depends on the time interval of the measurement and the initial conditions. We denote expectations under specific initial

conditions $\boldsymbol{c}(0)=0$, $\boldsymbol{u}(0)=e^{i\theta_0}$ by $\mathbb{E}_{\theta_0}[\cdot]$, and the expectation under a uniform distribution of θ_0 [still with $\boldsymbol{c}(0)=0$] by $\langle\cdot\rangle=\frac{1}{2\pi}\int\mathbb{E}_{\theta_0}[\cdot]d\theta_0$. Passage from $\mathbb{E}_{\theta_0}$ to $\langle\cdot\rangle$ is straightforward, as is the reverse. For example, for a set of variables $\boldsymbol{\xi},\ldots,\boldsymbol{\zeta}$ generically denoting any of $\boldsymbol{c},\boldsymbol{u}$, or $\boldsymbol{x}$ (not necessarily different), $\mathbb{E}_0$ can be obtained from $\langle\cdot\rangle$ using $\mathbb{E}_0[\boldsymbol{\xi}(t)\cdots\boldsymbol{\zeta}(t')^*]=\langle\boldsymbol{\xi}(t)\boldsymbol{u}(0)^*\cdots\boldsymbol{\zeta}(t')^*\boldsymbol{u}(0)\rangle$. Passage from $\mathbb{E}_0$ to $\mathbb{E}_{\theta_0}$ is then provided by the covariance of $\mathbb{E}_{\theta_0}$, that is, $\mathbb{E}_{\theta_0}[\boldsymbol{\xi}(t)\cdots\boldsymbol{\zeta}(t')^*]=\mathbb{E}_0[\boldsymbol{\xi}(t)\cdots\boldsymbol{\zeta}(t')^*]e^{-i(n-\bar{n})\theta_0}$, where n ($\bar{n}$) denotes the number of unconjugated (complex conjugated) variables among $\boldsymbol{\xi}(t),\ldots,\boldsymbol{\zeta}(t')^*$. Thus, $\langle\boldsymbol{\xi}(t)\cdots\boldsymbol{\zeta}(t')^*\rangle$ vanishes unless $n=\bar{n}$ since $\int_0^{2\pi}e^{-i(n-\bar{n})\theta_0}d\theta_0=\delta_{n\bar{n}}$. The expectation $\langle\cdot\rangle$ has two technical advantages over $\mathbb{E}_\theta[\cdot]$; it is time-translation invariant, assuming we only take differences of $\boldsymbol{c}$'s or $\boldsymbol{x}$'s, and it has the simple time-reversal property $\langle\boldsymbol{\xi}(t)\cdots\boldsymbol{\zeta}(t')^*\rangle=\langle\boldsymbol{\xi}(-t)^*\cdots\boldsymbol{\zeta}(-t')\rangle$.

For brevity, we label the time argument along the stroboscopic sampling sequence at multiples of T as an integer subscript, $\boldsymbol{\xi}_j:=\boldsymbol{\xi}(jT)$, and denote increments over one period as $\Delta\boldsymbol{\xi}_j:=\boldsymbol{\xi}((j+1)T)-\boldsymbol{\xi}(jT)$. The rotated increments $\widehat{\Delta\boldsymbol{\xi}}_j:=\Delta\boldsymbol{\xi}_j\,\boldsymbol{u}_j^*$ are of great value as they are independent and identically distributed. Therefore, $\widehat{\Delta\boldsymbol{\xi}}_j$'s are identically distributed and $\widehat{\Delta\boldsymbol{\xi}}_j$ is independent of $\widehat{\Delta\boldsymbol{\zeta}}_k$ for $j\neq k$. Thus, for $n\geqslant 1$, we have the reduction $\Delta\boldsymbol{\xi}_0^*\Delta\boldsymbol{\zeta}_n=\Delta\boldsymbol{\xi}_0^*\boldsymbol{u}_n\,\widehat{\Delta\boldsymbol{\zeta}}_n=(\Delta\boldsymbol{\xi}_0^*\boldsymbol{u}_1)(\mathcal{R}_1\cdots\mathcal{R}_{n-1})\widehat{\Delta\boldsymbol{\zeta}}_n$ into independent factors, where $\mathcal{R}_j:=\boldsymbol{u}_{j+1}\boldsymbol{u}_j^*$ is the rotation of the orientation from time jT to $(j+1)T$. Taking an expectation yields

$$\langle\Delta\boldsymbol{\xi}_0^*\Delta\boldsymbol{\zeta}_n\rangle=\langle\Delta\boldsymbol{\xi}_0^*\boldsymbol{u}_1\rangle\hat{C}^{n-1}\langle\widehat{\Delta\boldsymbol{\zeta}}_n\rangle,\tag{5}$$

where $\hat{C}:=\langle\mathcal{R}_j\rangle=C_{\boldsymbol{uu}^*}(T)=e^{-D_0T}=e^{-2\pi|\tau|}$. Using the time-reversal (TR) and time-translation (TT) invariances of $\langle\cdot\rangle$, the first factor on the right-hand side of Eq. (5) can be written as $\langle\Delta\boldsymbol{\xi}_0^*\boldsymbol{u}_1\rangle\overset{\text{TR}}{=}\langle(-\Delta\boldsymbol{\xi}_{-1})\boldsymbol{u}_{-1}^*\rangle\overset{\text{TT}}{=}-\langle\Delta\boldsymbol{\xi}_0\,\boldsymbol{u}_0^*\rangle=-\mathbb{E}_0[\Delta\boldsymbol{\xi}_0]$. Defining the one-period-increment expectation of $\boldsymbol{\xi}$ as

$$F_{\boldsymbol{\xi}}:=\mathbb{E}_0[\Delta\boldsymbol{\xi}_0]=\langle\Delta\boldsymbol{\xi}_0\,\boldsymbol{u}_0^*\rangle\equiv\langle\widehat{\Delta\boldsymbol{\xi}}_0\rangle,\tag{6}$$

we have

$$\langle\Delta\boldsymbol{\xi}_j^*\Delta\boldsymbol{\zeta}_{j+n}\rangle=-F_{\boldsymbol{\xi}}F_{\boldsymbol{\zeta}}\hat{C}^{n-1},\quad n\geqslant 1.\tag{7}$$

This shows more explicitly how the decays of all correlations are controlled by that of the orientation given in Eqs. (3). The one-period-increment expectations $F_{\boldsymbol{\xi}}$ are easy to obtain; $F_{\boldsymbol{u}}$, that of the orientation $\boldsymbol{u}$ with respect to the instantaneous center $\boldsymbol{c}$, follows from Eq. (3), $F_{\boldsymbol{x}}=iv\int_0^T C_{\boldsymbol{uu}^*}(t)dt$ for the motor position $\boldsymbol{x}$, and for the center $\boldsymbol{c}$, $F_{\boldsymbol{c}}$ follows from $F_{\boldsymbol{c}}+RF_{\boldsymbol{u}}=F_{\boldsymbol{x}}$:

$$F_{\boldsymbol{u}}=\hat{C}-1,\quad F_{\boldsymbol{x}}=\frac{RF_{\boldsymbol{u}}}{1+i\tau},\quad F_{\boldsymbol{c}}=\frac{-i\tau RF_{\boldsymbol{u}}}{1+i\tau}.\tag{8}$$

Covariances among all of the basic variables take the form

$$\begin{aligned}\langle(\boldsymbol{\xi}_n-\boldsymbol{\xi}_0)^*(\boldsymbol{\zeta}_n-\boldsymbol{\zeta}_0)\rangle&=\sum_{j=0}^{n-1}\sum_{k=0}^{n-1}\langle\Delta\boldsymbol{\xi}_j^*\Delta\boldsymbol{\zeta}_k\rangle\\&=\left[\langle\Delta\boldsymbol{\xi}_0^*\Delta\boldsymbol{\zeta}_0\rangle+2\frac{\mathrm{Re}\{F_{\boldsymbol{\xi}}F_{\boldsymbol{\zeta}}\}}{F_{\boldsymbol{u}}}\right]n\\&\quad+2(1-\hat{C}^n)\frac{\mathrm{Re}\{F_{\boldsymbol{\xi}}F_{\boldsymbol{\zeta}}\}}{F_{\boldsymbol{u}}^2}.\end{aligned}\tag{9}$$

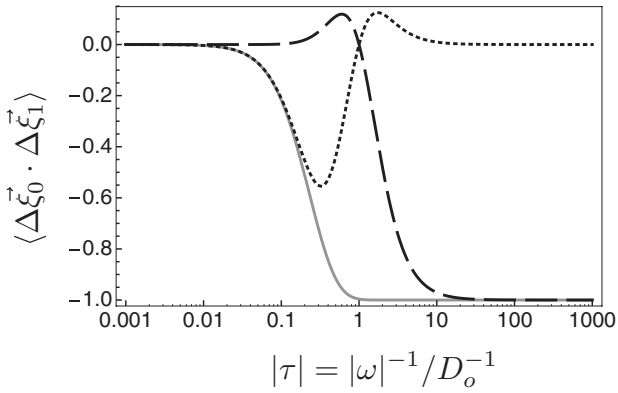

FIG. 3. One-period correlators $\langle\Delta\vec{\xi}_0\cdot\Delta\vec{\xi}_1\rangle=\mathrm{Re}\langle\Delta\boldsymbol{\xi}_0\Delta\boldsymbol{\xi}_1^*\rangle$ for $\boldsymbol{\xi}=\boldsymbol{u}$ (solid), $\boldsymbol{x}/R$ (dotted), and $\boldsymbol{c}/R$ (dashed). The mild anticorrelation for $\boldsymbol{x}/R$ at $|\tau|\lesssim 1$ and strong anticorrelation for $\boldsymbol{c}/R$ at $|\tau|\gg 1$ arise from deviations (from the asymptotic behavior) of the mean square increments across one period.

Note that the coefficient of n in Eq. (9) must be $4TD_{\text{eff}}$ when $\boldsymbol{\zeta}\in\{\boldsymbol{c},\boldsymbol{x}\}$, and zero if either $\boldsymbol{\xi}$ or $\boldsymbol{\zeta}$ is $\boldsymbol{u}$. Thus, $\langle\Delta\boldsymbol{u}_0^*\Delta\boldsymbol{\zeta}_0\rangle=-2\,\mathrm{Re}\{F_{\boldsymbol{\zeta}}\}$, across a single increment for $\boldsymbol{\zeta}\in\{\boldsymbol{u},\boldsymbol{c},\boldsymbol{x}\}$. Similarly, for both $\boldsymbol{\xi},\boldsymbol{\zeta}\in\{\boldsymbol{c},\boldsymbol{x}\}$, we obtain $\langle\Delta\boldsymbol{\xi}_0^*\Delta\boldsymbol{\zeta}_0\rangle=4TD_{\text{eff}}-2\,\mathrm{Re}\{F_{\boldsymbol{\xi}}F_{\boldsymbol{\zeta}}\}/F_{\boldsymbol{u}}$, combined with Eq. (9), yields

$$\frac{\langle(\boldsymbol{\xi}_n-\boldsymbol{\xi}_0)^*(\boldsymbol{\zeta}_n-\boldsymbol{\zeta}_0)\rangle}{nT}=4D_{\text{eff}}+\frac{2(1-\hat{C}^n)}{nT}\frac{\mathrm{Re}\{F_{\boldsymbol{\xi}}F_{\boldsymbol{\zeta}}\}}{F_{\boldsymbol{u}}^2}.\tag{10}$$

The first term on the right-hand side represents the diffusive contribution, and dominates the second term for long times.

Although one might expect correlations between successive increments to vanish in the limit of strong orientational diffusion ($|\tau|\to\infty$), they do not. The plots of $\mathrm{Re}\langle\Delta\boldsymbol{c}_0^*\Delta\boldsymbol{c}_1\rangle/R^2$, $\mathrm{Re}\langle\Delta\boldsymbol{x}_0^*\Delta\boldsymbol{x}_1\rangle/R^2$, and $\mathrm{Re}\langle\Delta\boldsymbol{u}_0^*\Delta\boldsymbol{u}_1\rangle$ shown in Fig. 3 reveal a strong *anticorrelation* between successive increments of $\boldsymbol{u}$ and $\boldsymbol{c}$. Surprisingly, it is strongest in the limit $|\tau|\to\infty$ for which the motion is most disordered. This phenomenon, as the gap between the dotted ($\boldsymbol{x}$) and dashed ($\boldsymbol{c}$) curves in Fig. 2, is related to the fact that $\boldsymbol{u}$ is trapped on a circle, $|\sum_{i=0}^n\Delta\boldsymbol{u}_i|\leqslant 2$. Hence, when the individual summands become large at large $|\tau|$, there must be strong anticorrelations.

Since stroboscopic sampling makes the deterministic rotary motion invisible, one might naively expect that it would not display any chirality. But it does, and it generates a *chiral diffusion*. Since $\boldsymbol{\xi}^*\boldsymbol{\zeta}=\vec{\xi}\cdot\vec{\zeta}+i\hat{\boldsymbol{z}}\cdot(\vec{\xi}\times\vec{\zeta})$ (where $\vec{\xi}$ is the vector counterpart of the complex number $\boldsymbol{\xi}$, and $\hat{\boldsymbol{z}}$ defines the plane of motion), the chirality manifests itself through the imaginary parts of correlators, $\hat{\boldsymbol{z}}\cdot\langle\vec{\xi}\times\vec{\zeta}\rangle=\Im\{\langle\boldsymbol{\xi}^*\boldsymbol{\zeta}\rangle\}$. For example, according to Eqs. (8),

$$\frac{\langle\Delta\boldsymbol{x}_0\,\boldsymbol{u}_0^*\rangle}{RF_{\boldsymbol{u}}}=\frac{1-i\tau}{1+\tau^2},\quad\frac{\langle\Delta\boldsymbol{c}_0\,\boldsymbol{u}_0^*\rangle}{RF_{\boldsymbol{u}}}=-\frac{(\tau+i)\tau}{1+\tau^2}.\tag{11}$$

If the chirality τ is positive (from the perspective of an observer sitting at the nanorotor's initial position $\boldsymbol{x}_0=R$ and facing in the direction of initial velocity $\boldsymbol{v}_0=iv$), then the expected position $\boldsymbol{x}(T)$ of the nanoparticle after one period is to the *left* and forward while the expectation of the instantaneous center $\boldsymbol{c}(T)$ is to the *right* and forward. Thus, the system engages in an unusual form of motion: a *chiral* stochastic

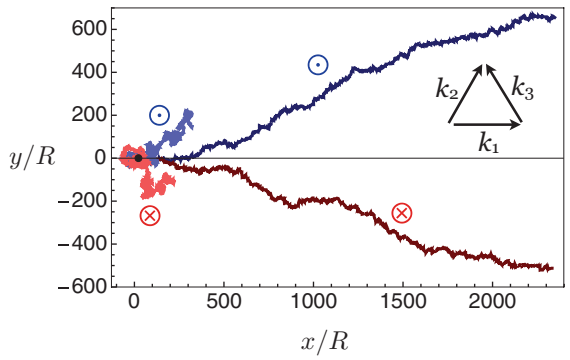

FIG. 4. (Color online) A potential $V = C_d \sum_{i=1}^{3} c_i \cos(\boldsymbol{k}_i \cdot \boldsymbol{x} + \delta_i)$ imparts an additional instantaneous velocity $-\nabla V/C_d$ onto the nanorotor, where C_d is the drag coefficient. For $c_1 = 0.3Rv$, $c_2 = c_3 = 0.18Rv$, $\delta_1 = \delta_2 = 0$, $\delta_3 = 1.3$ rad (and wave vectors of magnitude $3/R$ oriented as shown), V is chiral. The plot shows tracks over 10 000 nominal periods for orientational diffusers with $|\tau| = 0.5$: dark red for clockwise ($\otimes$) and dark blue for counterclockwise ($\odot$). Tracks for purely translational diffusers with the same (potential-free) effective diffusion coefficient are shown in light red and light blue for $\otimes$ and $\odot$, respectively.

diffusion. Experiments that seemed to show an effective attraction between counter-rotating nanorotors [18] will need to be reassessed to determine whether the observed "attraction" was an artifact of chiral diffusion. Furthermore, from Eq. (7), we obtain $\hat{z} \cdot \langle \Delta\vec{x}_j \times \Delta\vec{x}_{j+n} \rangle = 2\tau R^2 F_u^2 \hat{C}^{n-1}/(1+\tau^2)^2$. The positive proportionality to τ shows that the stroboscopically sampled path of the motor position has the same chirality as the deterministic motion. The distribution mean of $\boldsymbol{\xi}_n - \boldsymbol{\xi}_0$ is chirality dependent. Generally, $\langle (\boldsymbol{\xi}_n - \boldsymbol{\xi}_0)\boldsymbol{u}_0^* \rangle \overset{n\to\infty}{\longrightarrow} -F_\xi/F_u$ gives $\langle (\boldsymbol{x}_n - \boldsymbol{x}_0)\boldsymbol{u}_0^* \rangle \to -R/(1+i\tau)$ and $\langle (\boldsymbol{c}_n - \boldsymbol{c}_0)\boldsymbol{u}_0^* \rangle \to i\tau R/(1+i\tau)$. Again, the dependence on the sign of τ reflects chirality. The stroboscopically sampled rotor position $\boldsymbol{x}_n$ is *not* Markovian: A hidden orientational variable ($\boldsymbol{u}_n$) provides the memory for $\boldsymbol{x}_n$ to behave as a chiral persistent random walk with a surprising short-term drift that must be borne in mind during experimental analysis.

Chirality of motion can have particularly dramatic impact in the presence of a chiral *environment*. For example, consider a population of rotary nanomotors within a chiral periodic potential, moving according to overdamped dynamics (i.e., at low Reynolds number). Such a potential could be created by, e.g., a patterned substrate or an optical lattice. Our simulations demonstrate that this scenario generically produces a long-term chirality-dependent drift velocity as illustrated in Fig. 4.

Powered nanoscale motors are now a laboratory reality. Powered rotational motion combined with orientational diffusion produces an effective translational diffusion with an unusual chiral character. Recent advances in mechanisms for inducing rotary motion at the nanoscale [21,22] also suggest possible extensions of these phenomena to smaller length scales, particularly when the dynamics are compatible with orientational fluctuations and symmetry is broken to obtain orbital motions.

This work was supported by the NSF under Grant No. DMR-0820404 through the Penn State Center for Nanoscale Science.

[1] W. F. Paxton, S. Sundararajan, T. E. Mallouk, and A. Sen, Angew. Chem., Int. Ed. **45**, 5420 (2006).
[2] J. Wang and K. M. Manesh, Small **6**, 338 (2010).
[3] T. Mirkovic, N. S. Zacharia, G. D. Scholes, and G. A. Ozin, Small **6**, 159 (2010).
[4] J. Gibbs and Y. Zhao, Front. Mater. Sci. **5**, 25 (2011).
[5] S. J. Ebbens and J. R. Howse, Soft Matter **6**, 726 (2010).
[6] U. M. Córdova-Figueroa and J. F. Brady, Phys. Rev. Lett. **100**, 158303 (2008).
[7] J. R. Howse, R. A. L. Jones, A. J. Ryan, T. Gough, R. Vafabakhsh, and R. Golestanian, Phys. Rev. Lett. **99**, 048102 (2007).
[8] R. Golestanian, T. B. Liverpool, and A. Ajdari, New J. Phys. **9**, 126 (2007).
[9] E. Lauga, Soft Matter **7**, 3060 (2011).
[10] M. E. Cates, Rep. Prog. Phys. **75**, 042601 (2012).
[11] B. M. Friedrich and F. Jülicher, New J. Phys. **10**, 123025 (2008).
[12] E. Lauga, Phys. Rev. Lett. **106**, 178101 (2011).
[13] M. Ibele (unpublished).
[14] S. van Teeffelen and H. Löwen, Phys. Rev. E **78**, 020101 (2008).
[15] I. Sendiña-Nadal, S. Alonso, V. Pérez-Muñuzuri, M. Gómez-Gesteira, V. Pérez-Villar, L. Ramírez-Piscina, J. Casademunt, J. M. Sancho, and F. Sagués, Phys. Rev. Lett. **84**, 2734 (2000).
[16] D. Takagi, A. B. Braunschweig, J. Zhang, and M. J. Shelley, Phys. Rev. Lett. **110**, 038301 (2013).
[17] L. Qin, M. J. Banholzer, X. Xu, L. Huang, and C. A. Mirkin, J. Am. Chem. Soc. **129**, 14870 (2007).
[18] Y. Wang, S. to Fei, Y.-M. Byun, P. E. Lammert, V. H. Crespi, A. Sen, and T. E. Mallouk, J. Am. Chem. Soc. **131**, 9926 (2009).
[19] W. Paxton, K. Kistler, C. Olmeda, A. Sen, S. S. Angelo, Y. Cao, T. Mallouk, P. Lammert, and V. Crespi, J. Am. Chem. Soc. **126**, 13424 (2004).
[20] Y. Wang, R. M. Hernandez, D. J. Bartlett, J. M. Bingham, T. R. Kline, A. Sen, and T. E. Mallouk, Langmuir **22**, 10451 (2006).
[21] L. Vuković and P. Král, Phys. Rev. Lett. **103**, 246103 (2009).
[22] A. Prokop, J. Vacek, and J. Michl, ACS Nano **6**, 1901 (2012).